applied optics

Probability density function of the electric field in diffuse correlation spectroscopy of human bone *in vivo*

Tiziano Binzoni,[1,2,*] Bruno Sanguinetti,[3] Dimitri Van de Ville,[2,4] Hugo Zbinden,[3] and Fabrizio Martelli[5]

[1]Département de Neurosciences Fondamentales, University of Geneva, Switzerland
[2]Département de l'Imagerie et des Sciences de l'Information Médicale, University Hospital, Geneva, Switzerland
[3]Group of Applied Physics, University of Geneva, Switzerland
[4]Institute of Bioengineering, Ecole Polytechnique Fédérale de Lausanne (EPFL), Switzerland
[5]Dipartimento di Fisica e Astronomia dell'Università degli Studi di Firenze, Sesto Fiorentino, Firenze, Italy
*Corresponding author: tiziano.binzoni@unige.ch

Received 1 September 2015; revised 1 December 2015; accepted 8 December 2015; posted 10 December 2015 (Doc. ID 249178); published 22 January 2016

Diffuse correlation spectroscopy (DCS) is the technique of choice for non-invasive assessments of human bone blood flow. However, DCS classical algorithms are based on the fundamental assumption that the electric field of the light reaching the DCS photodetector is a zero-mean complex Gaussian variable. The non-validity of this hypothesis might produce inaccurate blood flow estimations. It is shown that for the human tibia, the "Gaussian hypothesis" holds for interoptode distances ≥20 mm. This lower boundary seems to depend on the type of investigated tissue.

OCIS codes: (170.0170) Medical optics and biotechnology; (170.3660) Light propagation in tissues; (170.3340) Laser Doppler velocimetry; (290.5825) Scattering theory.

http://dx.doi.org/10.1364/AO.55.000757

1. INTRODUCTION

Diffuse correlation spectroscopy (DCS) is an optical technique allowing, among other applications, the non-invasive assessment of mean tissue blood flow in humans [1–4]. In particular, DCS has the potential to become the instrument of choice in the investigation of the regulatory mechanisms of the bone neurovascular system in humans [5]. In fact, the study of bone blood flow regulation in humans has always been a challenging topic due to the difficulty of accessing this tissue with other known, often invasive, techniques.

It is essential to verify the conditions and range of validity of the mathematical algorithms utilized in combination with the DCS hardware for bone tissue to prevent potential physiological misinterpretations of the DCS data. In fact, at the core of the DCS algorithm, there is the well-known Siegert relation [6]:

$$g^{(2)}(\tau) = 1 + \beta|g^{(1)}(\tau)|^2, \quad (1)$$

where τ is a time delay and $0 \le \beta \le 1$. The function $g^{(1)}(\tau)$ is the normalized electric field autocorrelation function from which the blood flow values assessed by the DCS instrument are derived, and $g^{(2)}(\tau)$ is the normalized autocorrelation function of the photoelectric current. The function $g^{(1)}(\tau)$ is a quantity that would be extremely difficult to measure *in vivo*, while $g^{(2)}(\tau)$ is easily measurable experimentally by means of the DCS instrument. Equation (1) represents the link between $g^{(1)}(\tau)$, for which the DCS theory (mathematical model) allowing us to derive the blood flow is known, and the measurable quantity $g^{(2)}(\tau)$. Thus, the non- validity of Eq. (1) might induce errors in a blood flow estimation.

It is essential to note that Eq. (1) is derived by using the hypothesis that the electric field of the light coming out of the tissue is a zero-mean complex Gaussian variable [7–9]. We will call this hypothesis, from now on, the "Gaussian hypothesis" (GH). It is usually assumed [7–9] that, for this hypothesis to be true, photons scatter on moving scatterers and that moving scatterers are independent and numerous. Indeed, in order to have Gaussian statistics, the phases of the partial electric fields contributing to the total field at the detector must be sufficiently random. The scattering on static components must also be limited.

When biological tissues are under real experimental conditions, it is not clear when the moving scatterers (in this case, red blood cells) can be considered as "numerous." It must also be noticed that bone tissue has a lower blood content compared,

e.g., to skeletal muscle or the brain tissue, which further complicates the GH for this tissue. Tissues such as bone, skeletal muscle, and brain tissue have a "non-vascular" volume that may represent ~90% of the total tissue volume. Thus, the number of scattering events for a photon with static scatterers may actually be expected to be large compared to that of moving red blood cells. This might be another fact influencing the GH. Moreover, red blood cells move along a fixed network of fine capillaries, arterioles, and venules. This geometrical configuration clearly makes the movement not completely independent, as required by the GH.

In practice, there is a lack of literature on the validity of the GH in real bone tissue. For this reason, in the present contribution, two points have been considered: (1) test the GH by assessing the probability density function (pdf) of the electric field in human bone tissue, and (2) assess the pdf in an experimental setting comparable to that of a real DCS experiment to completely ensure that the results are applicable in these conditions. We hope that the present results will represent a further step in the development of DCS for the study of bone blood flow regulation in humans.

2. METHODS

A. Aim of the Work

The aim of the present work is to verify that the pdf of the electric field related to the light coming out of the tissue is Gaussian (normal distribution). The electric field cannot be measured with the experimental setting typical for DCS. However, the resulting instantaneous light intensity, I, can be measured with a photodetector. If the electric field is Gaussian, then the pdf of the number of photons I reaching a single-photon detector in a time interval Δt can be expressed as [10] (the symbols utilized here do not have the same meaning as in [10]):

$$p_{\mathrm{I}}(I) = \frac{1}{\mathcal{P}\bar{I}}\left\{\exp\left[-\frac{2I}{(1+\mathcal{P})\bar{I}}\right] - \exp\left[-\frac{2I}{(1-\mathcal{P})\bar{I}}\right]\right\}, \quad (2)$$

where $\mathcal{P} \in [0, 1]$ is the degree of polarization, and $\bar{I} > 0$ is the average I. In practice, it remains to be verified if in human bone the detected photons have a probability distribution that can be described by Eq. (2). If this is the case, then the GH is true and the Siegert relation [Eq. (1)] can be utilized to derive DCS blood flow values.

B. Experimental Setup

The main parts of the experimental setup consisted (see Fig. 1) of a 785 nm CW laser source (IRLD50, Moor Instruments Ltd.) with a coherence length >1 m and a photodetector. Considering the very low number of photons reaching the photodetector, especially for large interoptode distances such as $\rho = 30$ mm (see below), it was necessary to use a very sensitive photodetector. For this reason, we used a free-running, single-photon avalanche photodetector (SPAD) module running in the Geiger mode (ID 120, ID Quantique) with a quantum efficiency of $\eta = 0.8$ (i.e., 80%) at 785 nm, a large active sensor area of 500 μm diameter, and a dark count rate down to 30 Hz. The "global" dead time was of the order of 1 μs. A multimode optical fiber (core diameter 400 μm) was connected to the laser. Another 2 m (Huber Suhner) few-modes optical fiber (core diameter 9 μm) was connected to the SPAD. The acquisition software and data treatment were written in the MATLAB language (Mathworks Inc.). A counter (NI USB-6251, National Instruments Corporation) with a maximum count rate of 20 MHz was connected to the transistor–transistor logic output of the SPAD module. The photons were counted during 1025×1000 consecutive time intervals of duration $\Delta t = 12.5$ μs each (corresponding to a sampling frequency of $1/12.5\,\mu\mathrm{s}^{-1} = 80$ kHz). From these data, the pdf, $\hat{p}_{\mathrm{n}}(n)$, of the number of counts, n, counted in the time interval, Δt, was obtained. This operation was repeated 10 times to estimate the mean and the standard deviation of $\hat{p}_{\mathrm{n}}(n)$.

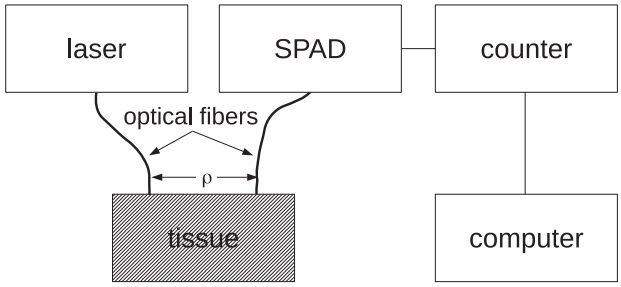

Fig. 1. Schematic drawing representing the experimental setup. The box "tissue" may represent *in vivo* measurements on a human tibia or forearm skeletal muscles. The parameter ρ is the interoptode distance.

C. Relating SPAD Counts to Actual Photon Numbers

In general, single-photon detectors similar to the one utilized in the present work are non-linear detectors. Thus, the number n obtained at the output of the counter does not correspond to the actual number I of photons reaching the photodetector during the time interval Δt. As is well known, the relationship linking I and n for the present SPAD configuration may be expressed by using the modified Mandel equation [11,12]:

$$p_{\mathrm{n}}(n) = \int_0^\infty p_{\mathrm{GP}}(n; \eta I, \lambda) p_{\mathrm{I}}(I)\mathrm{d}I, \quad (3)$$

where, for $\lambda < 0$ (see below),

$$p_{\mathrm{GP}}(n; \eta I, \lambda) = \frac{p^*_{\mathrm{GP}}(n; \eta I, \lambda)}{\sum_{n=0}^{\infty} p^*_{\mathrm{GP}}(n; \eta I, \lambda)}, \quad (4)$$

and where

$$p^*_{\mathrm{GP}}(n; \eta I, \lambda) = \begin{cases} \frac{\eta I(\eta I + n\lambda)^{n-1} e^{-(\eta I + n\lambda)}}{n!}; & n = 0, 1, 2, \cdots \\ 0; & n \geq n_o \end{cases}. \quad (5)$$

The pdf $p_{\mathrm{GP}}(n; \eta I, \lambda)$ is the generalized Poisson distribution (GP). In the GP distribution, the parameter λ defines the truncation n_o (integer) by the inequality $\max(-1, -\eta I/n_o) \leq \lambda < 1$. For $\lambda = 0$, Eq. (4) reduces the ordinary Poisson distribution with $n_o = \infty$.

We note that actually, Eq. (3) is very general, and other pdfs can be substituted for $p_{\mathrm{I}}(I)$ depending on the actual pdf of the light intensity reaching the detector. Thus, let us now study a particular case of an I pdf that will allow us to derive an explicit

analytical form for λ. As seen in Section 2.B, the SPAD utilized for measurements is an hybrid counter. In this case, the relationship between the photon number I in the constant regime (i.e., equivalent to replace for a while $p_I(x)$ by $\delta(x-I)$) and the mean photon number actually counted by the SPAD, $\langle n\rangle = \sum_n n p_n(n)$, is [13]:

$$\langle n\rangle = \frac{\eta I e^{-\frac{\eta I \tau_p}{\Delta t}}}{1+\frac{\eta I \tau_{np}}{\Delta t}}. \tag{6}$$

Here, the parameters τ_p and τ_{np} represent the paralyzable and non-paralyzable dead-time components of the hybrid counter. By following the method proposed in [14], it is possible to derive λ using (see the proposed approximation of Eq. (21) in [14])

$$p \approx \frac{\langle n\rangle^2}{I^2}, \tag{7}$$

and (see Eq. (22) in [14])

$$p = \frac{1}{(1-\lambda)^2}. \tag{8}$$

By combining Eqs. (6), (7), and (8):

$$\lambda = 1 - e^{\frac{\tau_p \eta I}{\Delta t}} - \frac{\tau_{np}\eta I}{\Delta t} e^{\frac{\tau_p \eta I}{\Delta t}}. \tag{9}$$

Equation (9) holds for any chosen I and can be utilized in general in Eq. (3). From Eq. (9), it follows that $\lambda \le 0$. As expected, when $\tau_p = 0$, λ holds for the special case of a non-paralyzable detector, and when $\tau_{np} = 0$, it holds for a paralyzable detector [12]. In summary, $p_n(n)$ [Eqs. (2) and (3)] represents the model for the experimental data $\hat{p}_n(n)$ (see Section 2.B).

D. Choice of Suitable Acquisition Time Δt

For the experimental $\hat{p}_n(n)$ data to be valid and compatible with the model $p_n(n)$, it is necessary that the value of Δt is small compared to the correlation time of the phenomenon that we want to study, which is represented by $g^{(2)}(\tau)$. This is equivalent to $\Delta t \ll 1/\Delta\nu$, where $\Delta\nu$ is the bandwidth of the light reaching the detector [11]. To check the goodness of the chosen Δt and give an estimation of $\Delta\nu$, an acquisition of 2014×100 consecutive time intervals of duration $\Delta t = 12.5$ μs each has been performed. Then, the power density spectrum was assessed on each 2014 points group, and 100 spectra were obtained. The mean power density spectrum, $S_n(\nu)$, was then derived. The $S_n(\nu)$ bandwidth gave an estimation of $\Delta\nu$. One can note that this is the classic procedure to obtain $S_n(\nu)$ utilized in laser-Doppler flowmetry, a companion technique of DCS; i.e., $S_n(\nu)$ and $g^{(2)}(\tau)$ are related by the Fourier transform [15,16].

E. Analyzing the "Gaussian" Hypothesis

The obtained experimental data $\hat{p}_n(n)$ were fitted using the model $p_n(n)$ represented by Eqs. (2) and (3). The unknown fitting parameters were $\bar{I}$, τ_p, and τ_{np}. The parameter $\mathcal{P}$ was set to $\mathcal{P} = 0$ (see Section 4) by taking the limit $\mathcal{P} \to 0^+$ in Eq. (2). In practice, when $p_n(n)$ does not fit the data, the underlying electric field is not "Gaussian." Considering that the present results appear to be clear even without a sophisticated analysis, a simple criterion for the goodness of fit was chosen by using the relative squared error:

$$\varepsilon_{rel} = \frac{\sum_{n=1}^{max}[p_n(n)-\hat{p}_n(n)]^2}{\sum_{n=1}^{max}[\bar{p}_n-\hat{p}_n(n)]^2}, \tag{10}$$

where

$$\bar{p}_n = \frac{1}{n_{max}}\sum_{n=1}^{n_{max}}\hat{p}_n(n), \tag{11}$$

and where n_{max} is the maximum n for which $\hat{p}_n(n)$ was not nil. The level at which the electric field was reasonably considered not to be "Gaussian," and thus where the GH would not hold, was set to the heuristic value $\varepsilon_{rel} > 0.03$ (see Section 3). The fitting has been performed by imposing the constraint >0 to $\bar{I}$, τ_p, and τ_{np}.

F. Experimental Protocol

Three sets of measurements were implemented with the purpose of studying the validity of the GH in a typical measurement configuration (set 1) for a range of source-detector distances (set 2) and for different red blood cells' tissue contents (set 3). In the following, the three sets are described.

1. Measurements: Set 1

The first set of demonstrative measurements was realized on the tibias of 6 male subjects. In this case, the subject was comfortably seated on a chair with his feet resting on an elevated support the same height of the chair. The optodes were placed on the right tibial diaphysis (medial surface) at the half distance between the medial malleolus and the medial condyle, along the main axis of the tibia. The interoptode distance was $\rho = 20$ mm. One data acquisition following the procedure presented in Section 2.B was realized for each subject (duration ~12 min) in order to obtain the 10 $\hat{p}_n(n)$ curves.

To ensure the reliability of the choice made for the Δt value, an $S_n(\nu)$ spectrum has been acquired for each subject as explained in Section 2.D. The optodes were placed in the same position as for the $\hat{p}_n(n)$ acquisition.

2. Measurements: Set 2

A second set of 5 $\hat{p}_n(n)$ measurements (10 $\hat{p}_n(n)$ curves each) was performed on the tibia of one subject. However, in this case, the interoptode distances were $\rho \in \{10, 15, 20, 25, 30\}$. This to evaluate if the different mean path lengths traveled by the photons through the tissue may influence the GH.

3. Measurements: Set 3

To investigate if different red blood cells' tissue contents might influence the validity of the GH, a series of $\hat{p}_n(n)$ acquisitions was performed as in Section F.2, but, this time, they were performed on the forearm muscles of one subject. In fact, skeletal muscle has a higher concentration of red blood cells than bone tissue. Intuitively, we can compare the absorption coefficient of skeletal muscle (~0.025 mm^{-1} [17]) to that of the bone (~0.005 mm^{-1} [18]), which is roughly related to the red blood cells' tissue contents. In this case, the subject was seated on a chair with the right forearm comfortably placed over the optodes and with the hand in the prone position. The optodes were positioned along the *brachioradialis* muscle, where the forearm has the largest diameter.

3. RESULTS

A. Measurements: Set 1

The $S_n(\nu)$ for 6 subjects, measured on the tibia, are shown in Fig. 2. A sampling frequency of 80 kHz (i.e., a sampling time of $\Delta t = 12.5$ μs) is sufficient to satisfy the Nyquist sampling criterion and cover the whole spectrum. The bandwidth is at the half height in the range $\Delta\nu \in [1.56, 3.91]$ kHz. Thus, the relationship $\Delta t \ll 1/\Delta\nu$ (see Section 2.D) is satisfied for all subjects, as advocated in [11]. This kind of spectra is also typically found in laser-Doppler flowmetry, and further confirms that the experimental setup allows us to successfully perform the proposed experiment.

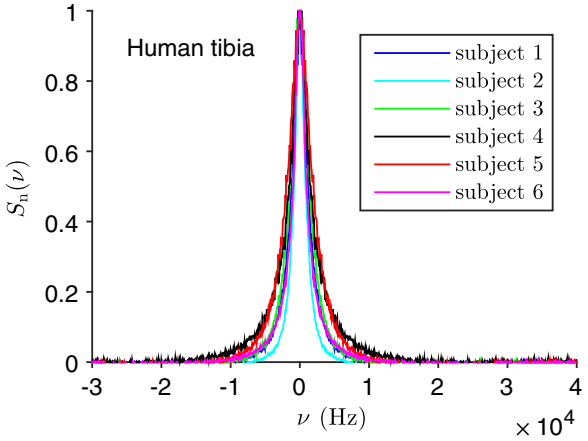

Fig. 2. Power density spectra, $S_n(\nu)$, for $\rho = 20$ mm. To better show the ν bandwidth, the spectra have been baseline corrected and normalized to 1.

In Figs. 3(a)–3(f) are shown the experimental pdfs, $\hat{p}_n(n)$ for 6 subjects, with the relative fitted model, $p_n(n)$. In Fig. 3(g), all the curves satisfy the GH, because $\varepsilon_{rel} < 0.03$ (see Section 2.E). Thus, in this case, one can reasonably say that the relative electric fields are Gaussian, and that the Siegert relation [Eq. (1)] is valid for this experimental configuration.

B. Measurements: Set 2

In Fig. 4, we report the $\hat{p}_n(n)$ data from one subject for different ρ values, with the relative fitted curves $p_n(n)$. It clearly appears that too-short $\rho < 20$ infirm the GH hypothesis (i.e., $\varepsilon_{rel} > 0.03$).

C. Measurements: Set 3

In Fig. 5, the same experimental protocol as in Fig. 4 has been applied; however, in this case, the measurements have been performed on skeletal muscle. It appears that in this case, the GH holds for smaller ρ values, i.e., starting from $\rho \geq 15$ mm compared to $\rho \geq 20$ mm for bone. Due to the higher absorption coefficient of skeletal muscle compared to bone tissue, all curves are globally displaced to lower n values [compare Figs. 5(a) and 4(a)].

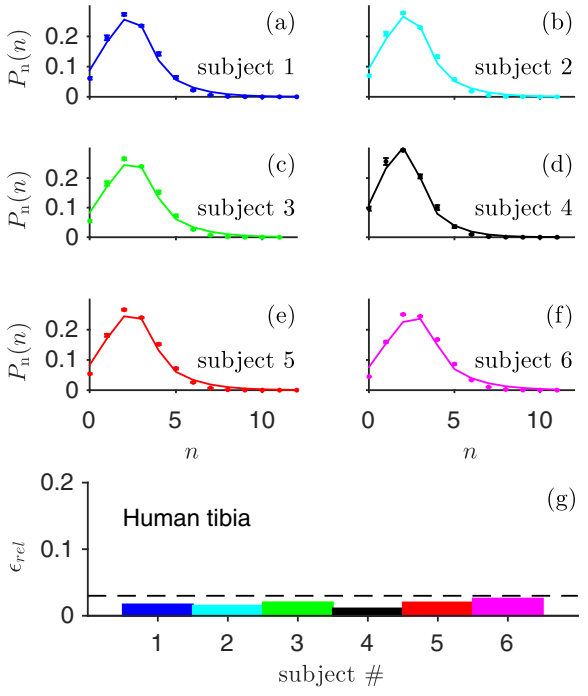

Fig. 3. Dots: experimental pdfs, $\hat{p}_n(n)$, for $\rho = 20$ mm. Vertical bars are standard deviations. Continuous lines: fitted model $p_n(n)$ [Eqs. (2) and (3)]. The relative errors between the experimental and fitted data are reported in panel (g). The horizontal dashed line represents $\varepsilon_{rel} = 0.03$.

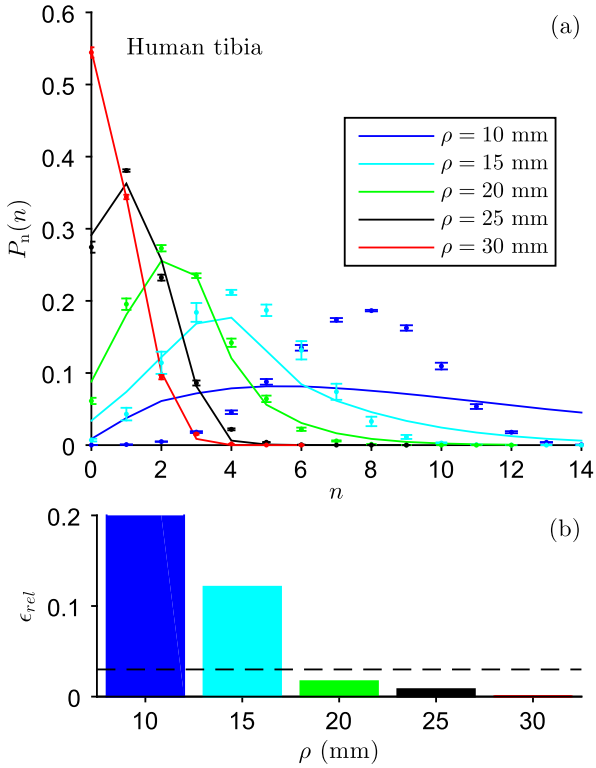

Fig. 4. Dots: experimental pdfs, $\hat{p}_n(n)$, for one subject and different ρ values. Vertical bars are standard deviations. Continuous lines: fitted model $p_n(n)$ [Eqs. (2) and (3)]. The relative errors, ε_{rel}, between the experimental and fitted data are reported in panel (g). For readability reasons, the ε_{rel} value at $\rho = 10$ mm is out of axis. The actual value is $\varepsilon_{rel} \approx 0.68$. The horizontal dashed line represents $\varepsilon_{rel} = 0.03$.

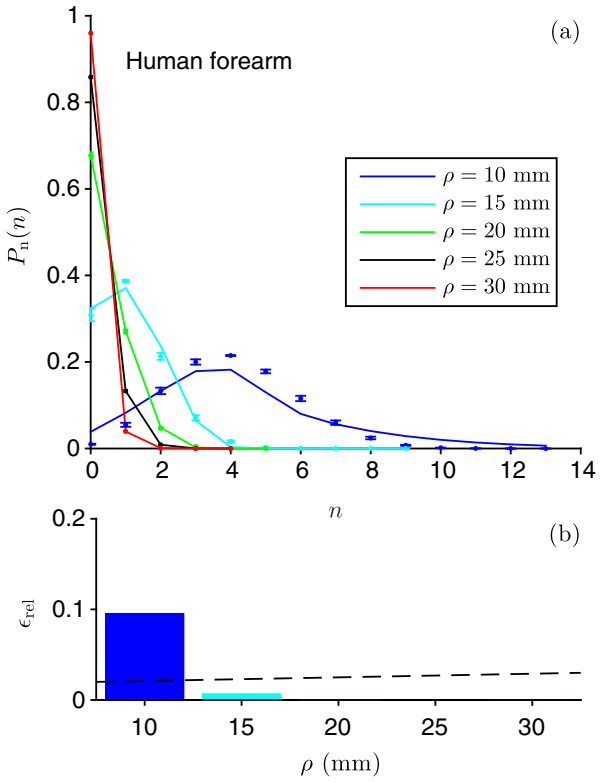

Fig. 5. Dots: experimental pdfs, $\hat{p}_n(n)$, for one subject and different ρ values. Vertical bars are standard deviations. Continuous lines: fitted model $p_n(n)$ [Eqs. (2) and (3)]. The relative errors, ϵ_{rel}, between the experimental and fitted data are reported in panel (g). Some bars are not visible because their values are too small. The horizontal dashed line represents $\epsilon_{rel} = 0.03$.

4. DISCUSSION AND CONCLUSIONS

In the present contribution, we have investigated the GH, which the validity of the Siegert relation [Eq. (1)] depends on in different typical experimental configurations. To this purpose, we hypothesized that the light coming out from the tissue is completely unpolarized, i.e., $P = 0$ in Eq. (2) (see Section 2.E). This is a very reasonable and usually accepted assumption. In fact, the shortest path length traveled by the photons inside the tissue corresponds by definition to the interoptode distance. In the present measurements, ρ was always $\geq$10 mm and thus, due to the optical properties of bone or skeletal muscle, the light was completely unpolarized when it reached the SPAD [19,20]. In practice, values $P > 0$ produce fitted $p_n(n)$-curves that are worse (results not shown). Actually, this is not surprising, because when P increases from 0 to 1, the $p_n(n)$ curves generated by Eq. (3) become more and more monotonically decreasing curves (i.e., "exponential-like" decreasing curves). This kind of shape obviously cannot fit the curves appearing, e.g., in Fig. 3.

The GH hypothesis on the electric field has been tested by studying the probability density function of the photons. In fact, the electric field cannot be easily measured *in vivo*, and thus the desired information has be extracted from the probability density function of the photons.

It is interesting to note, as one of our referees pointed out, that a very careful study of the behavior of the parameter β (see e.g., [21]) might allow us to infer some conclusions on the validity of the GH, i.e., β values lower than the one predicted theoretically would weaken the GH [22].

Thus, in the present contribution, we have shown that the GH is not always true. In particular, in human tibias, the GH appears to be valid only for $\rho \geq 20$ mm. In skeletal muscle, probably due to the higher content of red blood cells, and thus to the higher number of scattering events of photons with moving scatterers, the GH seems to be valid for smaller ρ values. The important point here is that, in general, in DCS, the GH should be tested before applying Eq. (1) at short interoptode distances. In fact, the non-validity of the GH might introduce undesirable errors in the estimated blood flow values.

REFERENCES

1. D. A. Boas, L. E. Campbell, and A. G. Yodh, "Scattering and imaging with diffusing temporal field correlations," Phys. Rev. Lett. **75**, 1855–1858 (1995).
2. T. Durduran, R. Choe, W. B. Baker, and A. G. Yodh, "Diffuse optics for tissue monitoring and tomography," Rep. Prog. Phys. **73**, 076701 (2010).
3. M. Ninck, M. Untenberger, and T. Gisler, "Diffusing-wave spectroscopy with dynamic contrast variation: Disentangling the effects of blood flow and extravascular tissue shearing on signals from deep tissue," Biomed. Opt. Express **1**, 1502–1513 (2010).
4. M. Diop, K. Verdecchia, T.-Y. Lee, and K. S. Lawrence, "Calibration of diffuse correlation spectroscopy with a time-resolved near-infrared technique to yield absolute cerebral blood flow measurements," Biomed. Opt. Express **2**, 2068–2081 (2011).
5. T. Binzoni and L. Spinelli, "Near-infrared photons: A non-invasive probe for studying bone blood flow regulation in humans," J. Physiol. Anthropol. **34**, 28 (2015).
6. H. Z. Cummins and H. L. Swinney, "Light beating spectroscopy," in *Progress in Optics*, E. Wolf, ed. (North-Holland, 1970), Vol. **8**, pp. 133–200.
7. D. Pine, D. Weitz, J. Zhu, and E. Herbolzheimer, "Diffusing-wave spectroscopy: Dynamic light scattering in the multiple scattering limit," J. Phys. France **51**, 2101–2127 (1990).
8. P. Lemieux and D. Durian, "Investigating non-Gaussian scattering processes by using nth-order intensity correlation functions," J. Opt. Soc. Am. A **16**, 1651–1664 (1999).
9. C. Zhou, "*In vivo* optical imaging and spectroscopy of cerebral hemodynamics," Ph.D. thesis (University of Pennsylvania, 2007).
10. J. W. Goodman, *Statistical Optics* (Wiley Classics Library, 2000).
11. L. Mandel, "Fluctuations of light beams," in *Progress in Optics*, E. Wolf, ed. (North-Holland, 1963), Vol. **II**, pp. 181–248.
12. V. Kornilov, "Effects of dead time and afterpulses in photon detector on measured statistics of stochastic radiation," J. Opt. Soc. Am. A **31**, 7–15 (2014).
13. L. Neri, S. Tudisco, F. Musumeci, A. Scordino, G. Fallica, M. Mazzillo, and M. Zimbone, "Note: dead time causes and correction method for single photon avalanche diode devices," Rev. Sci. Instrum. **81**, 086102 (2010).
14. V. G. Kornilov, "A statistical description of the non-linearity of photon counts," Astron. Rep. **52**, 70–78 (2008).
15. T. Binzoni, D. Van De Ville, and B. Sanguinetti, "Time-domain algorithm for single-photon laser-Doppler flowmetry at large interoptode spacing in human bone," Appl. Opt. **53**, 7017–7024 (2014).
16. T. Binzoni and F. Martelli, "Assessing the reliability of diffuse correlation spectroscopy models on noise-free analytical Monte Carlo data," Appl. Opt. **54**, 5320–5326 (2015).
17. A. Torricelli, V. Quaresima, A. Pifferi, G. Biscotti, L. Spinelli, P. Taroni, M. Ferrari, and R. Cubeddu, "Mapping of calf muscle oxygenation and haemoglobin content during dynamic plantar flexion exercise

by multi-channel time-resolved near-infrared spectroscopy," Phys. Med. Biol. **49**, 685–699 (2004).
18. P. Farzam, P. Zirak, T. Binzoni, and T. Durduran, "Pulsatile and steady-state hemodynamics of the human patella bone by diffuse optical spectroscopy," Physiol. Meas. **34**, 839–857 (2013).
19. P. Bruscaglioni, G. Zaccanti, and Q. Wei, "Transmission of a pulsed polarized light beam through thick turbid media: Numerical results," Appl. Opt. **32**, 6142–6150 (1993).
20. S. Alali, M. Ahmad, A. Kim, N. Vurgun, M. F. Wood, and I. A. Vitkin, "Quantitative correlation between light depolarization and transport albedo of various porcine tissues," J. Biomed. Opt. **17**, 045004 (2012).
21. G. Dietsche, M. Ninck, C. Ortolf, J. Li, F. Jaillon, and T. Gisler, "Fiber-based multispeckle detection for time-resolved diffusing-wave spectroscopy: Characterization and application to blood flow detection in deep tissue," Appl. Opt. **46**, 8506–8514 (2007).
22. I. Flammer, G. Bucher, and J. Rička, "Diffusive wave illumination: Light-scattering study of colloidal dynamics in opaque media," J. Opt. Soc. Am. A **15**, 2066–2077 (1998).